6 Jun 88 Conference Presentation

Visualization and Anemometry of Forced Unsteady Flows About an X-29 Model

TA 2307-F1-38

J. Ashworth, T. Mouch, M. Luttges

F.J. Seiler Research Laboratory
USAF Academy CO 80840-6528

FJSRL-PR-90-0011

Distribution Unlimited

Numerous investigations on forced unsteady flows and associated lift enhancements suggest significant aerodynamic utility. To demonstrate the application potential of unsteady flow technology, an investigation comparing flow visualization and hotwire velocity measurements of the flow about an X-29 model was accomplished. Precious flow visualization has qualitatively defined the flow structures, and comparisons with quantitative hotwire anemometry data provides insight into the aerodyanmic enhancement of these forced unsteady flows. Flow visualization shows intricate interactions between the wingtip and leading edge vortices on the surface of the canard. These structures convect downstream and influence the flow patterns about the wing. Hotwire velocity measurements were taken above and below the wing, adding a quantitative dimension to understanding these flows. The unsteady flow phenomena show significant benefits that can be used to enhance the aerodynamic agility of maneuvering aircraft.

hot wire anemometers
canard configurations
vortices

12

UNCLASSIFIED UNCLASSIFIED UNCLASSIFIED NONE

AIAA'88

AIAA-88-2570-CP
Visualization and Anemometry Analysis of Forced Unsteady Flows About an X-29 Model

J. Ashworth, T. Mouch and M. Luttges, U.S. Air Force Academy, Colorado Springs, CO

AIAA 6th Applied Aerodynamics Conference

June 6-8, 1988/Williamsburg, Virginia

88-2570-CP

VISUALIZATION AND ANEMOMETRY ANALYSES OF FORCED UNSTEADY FLOWS ABOUT AN X-29 MODEL

J. Ashworth*, T. Mouch** and M. Luttges***
HQ USAFA/DFAN
U. S. Air Force Academy
Colorado Springs, Colorado 80840-5701

ABSTRACT

Over the past few years, numerous experimental and theoretical investigations on forced unsteady flows and associated lift enhancements have produced results suggestive of significant aerodynamic utility. To demonstrate the application potential of unsteady flow technology, an investigation comparing flow visualization and hotwire velocity measurements of the flow about an X-29 model was accomplished. The flow about the X-29 model is very complex due to the unique geometry of the model. This three-dimensional complexity is seen in static (nonoscillating canard) tests and is increased when the canard is driven through sinusoidal motions. Previous flow visualization investigations have qualitatively defined these flow structures, and comparisons with quantitative hotwire anemometry data provides insight into the aerodynamic enhancement characteristics of these forced unsteady flows. The unsteady flow visualization data show intricate interactions between the wingtip and leading edge vortices on the surface of the canard. These structures convect downstream and influence the flow patterns about the wing. Hotwire velocity measurements were taken above and below the surface of the tandem wing for identical canard dynamic conditions. These velocity profiles add a quantitative dimension to understanding these flows. Several hypotheses formed during purely visualization investigations have been supported. The unsteady flow phenomena show significant benefits that can be used to enhance the aerodynamic agility of maneuvering aircraft.

*Major, USAF
Associate Professor, Department of Aeronautics, U. S. Air Force Academy, Colorado Springs, Co.
Member AIAA

**Captain, USAF
Instructor, Department of Aeronautics, U. S. Air Force Academy, Colorado Springs, Co.
Member AIAA

***Professor, Department of Aerospace Engineering Sciences, University of Colorado, Boulder, Co.
Member AIAA

NOMENCLATURE

AOA	Model angle of attack
c	Canard chordlength measured at midspan
K	Nondimensional reduced frequency parameter, $K = \omega c/2V_\infty$
V_∞	Freestream tunnel velocity
α	Canard angle of attack (degrees)
α_m	Mean angle of attack (degrees)
α_ω	Oscillation amplitude (degrees)
ϕ	Nondimensional oscillation phase angle (% of the cycle beginning at α_{max})
ω	Rotational frequency in radians per second

INTRODUCTION

Enhancement of the low speed agility of maneuvering aircraft appears feasible through the application of forced unsteady flows. Investigations on two-dimensional airfoils[1-6] and three-dimensional wings[7-14] have advanced unsteady flow technology and indicate possible applications of these phenomena to actual aircraft. Initial studies with an advanced aircraft model[15] have verified this possibility and have indicated areas of effective application. Since the X-29 aircraft with canard and forward swept wing appears ideal for this unsteady flow application[16], a reflection-plane model of this aircraft was used for these studies. The X-29 canard and tandem wing configuration may prove to be a control surface combination that will allow tests of maximized unsteady flow effects[17] and enhanced aircraft maneuverability.

All aircraft are inherently three-dimensional and an understanding of the interactions between conventional leading edge and wingtip vortices produced about a surface is essential in applying the technology of unsteady aerodynamics to complete aircraft. Also, the vortical structures produced by a forward control surface will influence the flow about any trailing surfaces. Such previously

unstudied flow interactions are the subject of this investigation.

Due to the tactical situation, combat aircraft often must perform in flight regimes below ideal maneuvering airspeed (referenced in numerous Air Force Fighter Weapons School texts and publications). In this region of the aircraft flight envelope, the utilization of unsteady aerodynamics for lift enhancement and flow control may augment maneuvering characteristics and complement point-and-shoot capabilities.

METHODS

A 1/10 scale, reflection-plane model of the X-29 aircraft (Fig. 1A) was tested in a low speed wind tunnel at the University of Colorado[15]. The initial data were collected using a smokewire flow visualization technique[15] that illustrated detailed flow characteristics. The flow was visualized along vertical data planes carefully generated to pass at various spanwise locations across the canard and wing of the model. These tests were conducted with a tunnel velocity of 25 feet per second and with the canard oscillating through sinusoidal motions at a nondimensional reduced frequency of 1.0. The hotwire anemometry experiments utilized identical oscillating conditions. The visualizations and velocity measurements were recorded with a canard mean angle of attack of 15 degrees and an oscillation amplitude of $\pm$10 degrees. Additional evaluations were conducted with a mean angle of 12 degrees and an oscillation amplitude of $\pm$2 degrees. A comparison of the flow visualization and hotwire velocity data is made using identical spatial and temporal references for both data sets.

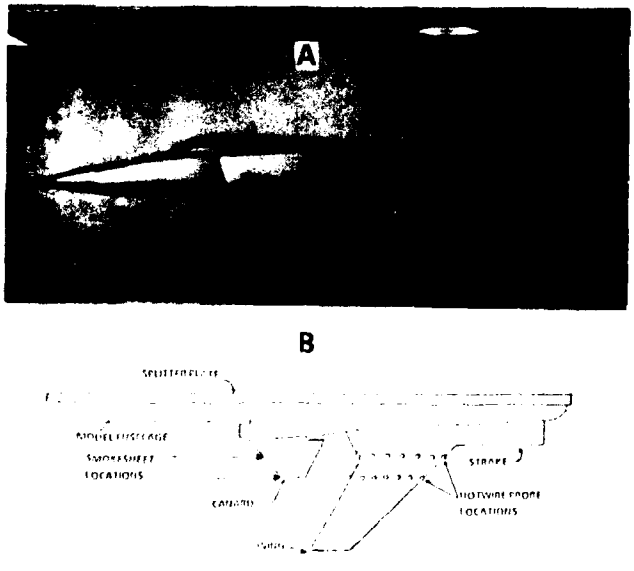

Fig. 1A/B Model photograph and planform with smoke locations.

The hotwire velocity data was collected and computer averaged for ten sample runs over two oscillation cycles. The data was plotted at each hotwire position for two complete cycles to ensure repeatability. The nondimensional oscillation phase angle, ϕ, is equal to 0.0 when the canard was at maximum angle of attack and equal to 1.0 when the canard had passed through the lower angles and returned to the maximum angle. The local hotwire velocity is plotted using the freestream velocity as a reference base. The hotwire probe stations were located in the same vertical (parallel to the freestream) planes as the flow visualization data (Fig 1B). Two vertical plane locations were studied: one across the midchord of the canard and one at the tip of the canard. For each vertical plane, four horizontal planes were chosen for data collection: one inch and two inches above the leading edge of the wing, and one inch and two inches below the leading edge of the wing. At each of these horizontal planes a chordwise mapping was conducted which included seven points equally spaced from leading to trailing edge (Fig 1B).

Due to the geometric complexity of the flow patterns about the X-29 model, qualitative as well as quantitative analyses were somewhat difficult. To allow realistic evaluations of the effects of forced unsteady motions, tests were performed using static (canard with fixed angle of attack) and dynamic (sinusoidally oscillating canard) conditions. The static tests were performed with the setting of the canard angle of attack ranging from 0 to 40 degrees. The model angle of attack (AOA) for all tests was set at 5 degrees relative to the tunnel freestream plane. The canard angle of attack was referenced to the centerline of the model. Each test condition included an analysis of static and dynamic results for both data collection techniques.

RESULTS

The spanwise locations about the X-29 model previously visualized using smoke wire techniques are shown in Fig. 1B. Since the unsteady flows generated by the oscillating canard affect the airflow about both the canard and the tandem wing of this model, hotwire analyses were first initiated about the wing using dynamic and spatial parameters identical to those used previously to acquire flow visualization data. The hotwire probe positions above and below the wing were chosen in plane with the smoke sheets. Using six equal increments across the chord of the wing, a quantitative picture was constructed showing the velocity magnitudes of the flow field about the wing.

To demonstrate three-dimensional characteristics and provide comparative insight, Fig. 2 depicts flow visualization

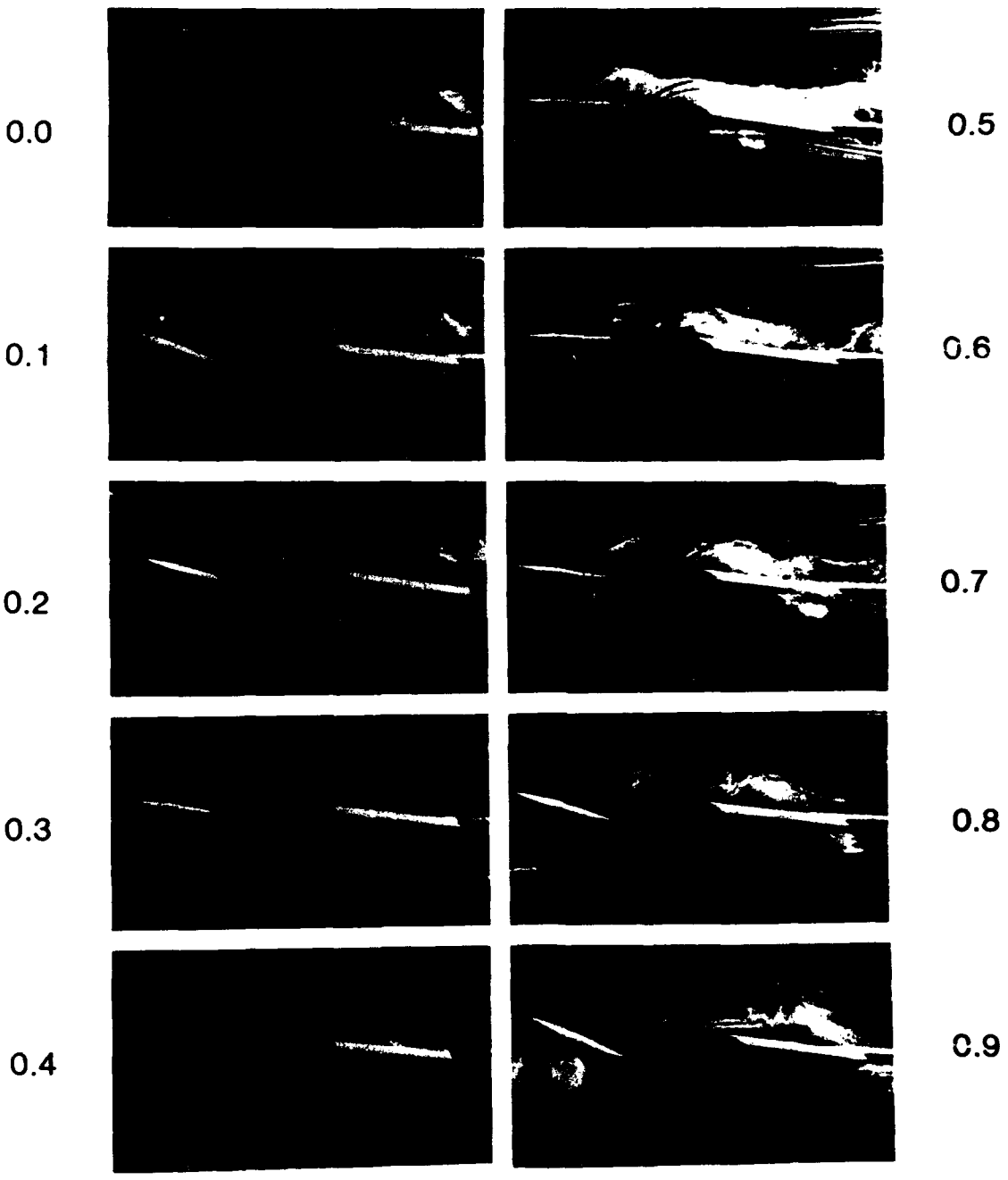

Fig. 2 Flow visualization of one complete pitching cycle, smoke sheet at the canard tip.

data for one complete oscillation cycle of the canard of the X-29 model. The smoke sheet is introduced in the vertical plane of the canard tip and is observed passing about the upper and lower surfaces of the wing. Throughout one cycle, the formation, shedding and convection of a composite wingtip and connected leading edge vortex is shown. For the first part of the cycle, ϕ = 0.0 to 0.2, a strong tip vortex is formed on the canard and convects downstream with the flow to a position at the leading edge of the wing. As the cycle continues, ϕ = 0.3 to 0.9, this canard tip vortex is divided by the leading edge with a portion of the vortex observed passing above and another, below the wing. At ϕ = 0.3 and 0.4, the tip vortex at the canard diminishes in size and the smoke is entrained in the canard leading edge vortex. The canard leading edge vortex is observed convecting across the top surface of the canard. It then traverses into the canard wake and passes well above the top of the wing. The combination of canard tip and leading edge

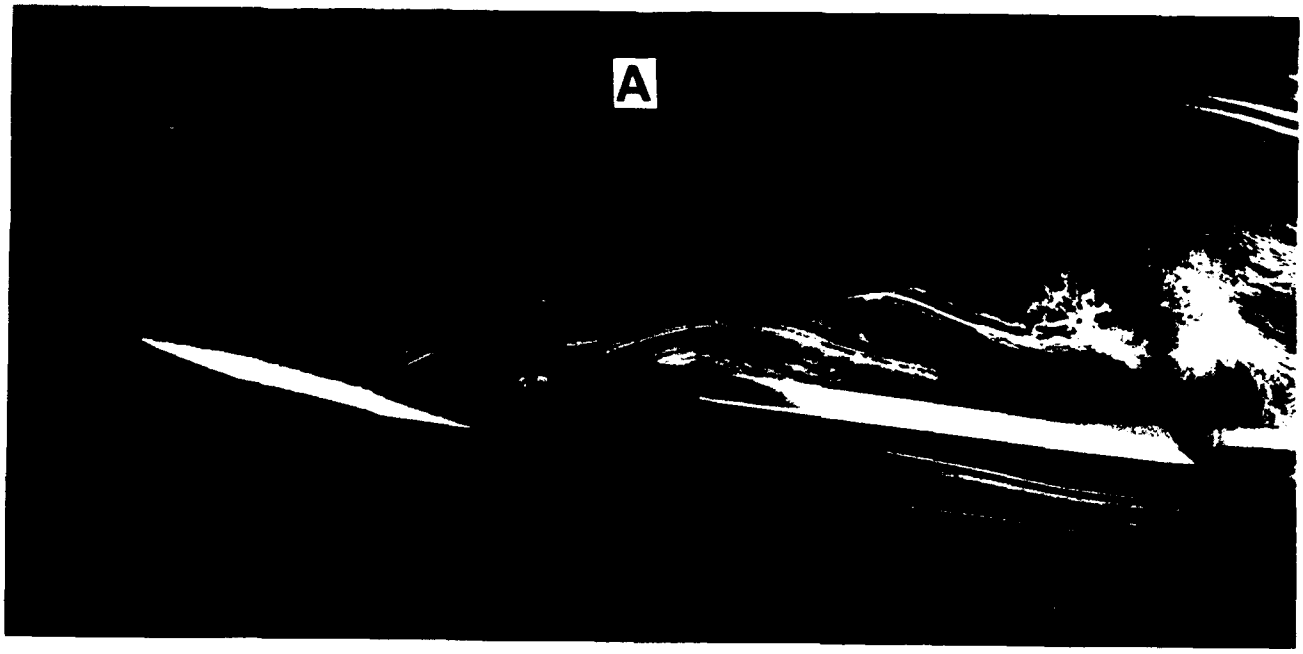

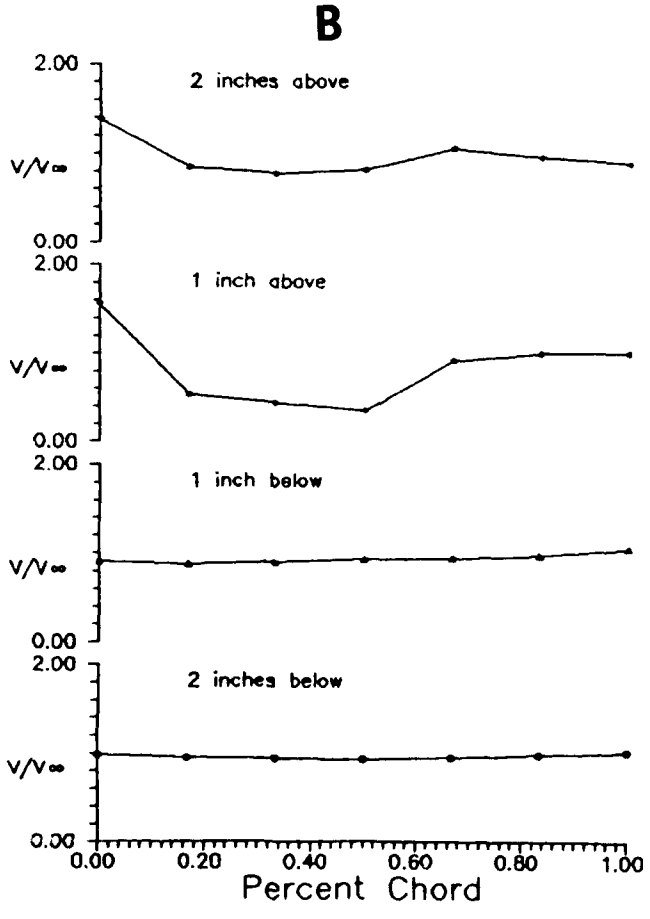

Fig. 3A/B Visualization patterns and velocity fluctuations for the vertical plane at the canard tip and ϕ = 0.2.

vortex convection across the surfaces of the wing creates a complex, three-dimensional flow pattern. To comprehend the effects of these visualized cyclic flow patterns about the wing, quantitative velocity measurements are essential.

Flow visualization and velocity fluctuations collected for different chord positions on the wing are shown in Fig. 3A/B. In the A portion of this figure, an instantaneous flow visualization photograph depicts the flow patterns about the canard and wing for ϕ = 0.2 in the canard oscillation cycle. The B portion shows the correlated instantaneous velocity recorded at each hotwire probe station for this point in the cycle. The hotwire stations are in horizontal planes one inch and two inches above and below the surface of the wing. The instantaneous velocities are plotted at each chordwise hotwire probe station with the tunnel freestream velocity as the horizontal baseline. These velocities record the effects of the unsteady flow vortices produced by the oscillating canard. The hotwire probe, itself, was positioned orthogonally to the oncoming flow.

The visualization photograph shows the canard tip vortex impinging on the leading edge of the wing and being split into two parts, one passing above and one passing below the wing. The canard leading edge vortex from the previous cycle can be seen convecting downstream as a near-circular rotational pattern located well above the trailing edge of the wing. The velocity plots for the upper surface trace some of the effects of canard tip vortex impingement on the wing surface. At the wing leading edge, the peak velocities at both one inch and two inches above the surface are nearly one and one-half times the freestream velocity. However, at the next three chordwise locations, the velocities drop well below the freestream value. These low velocities appear to be representative of

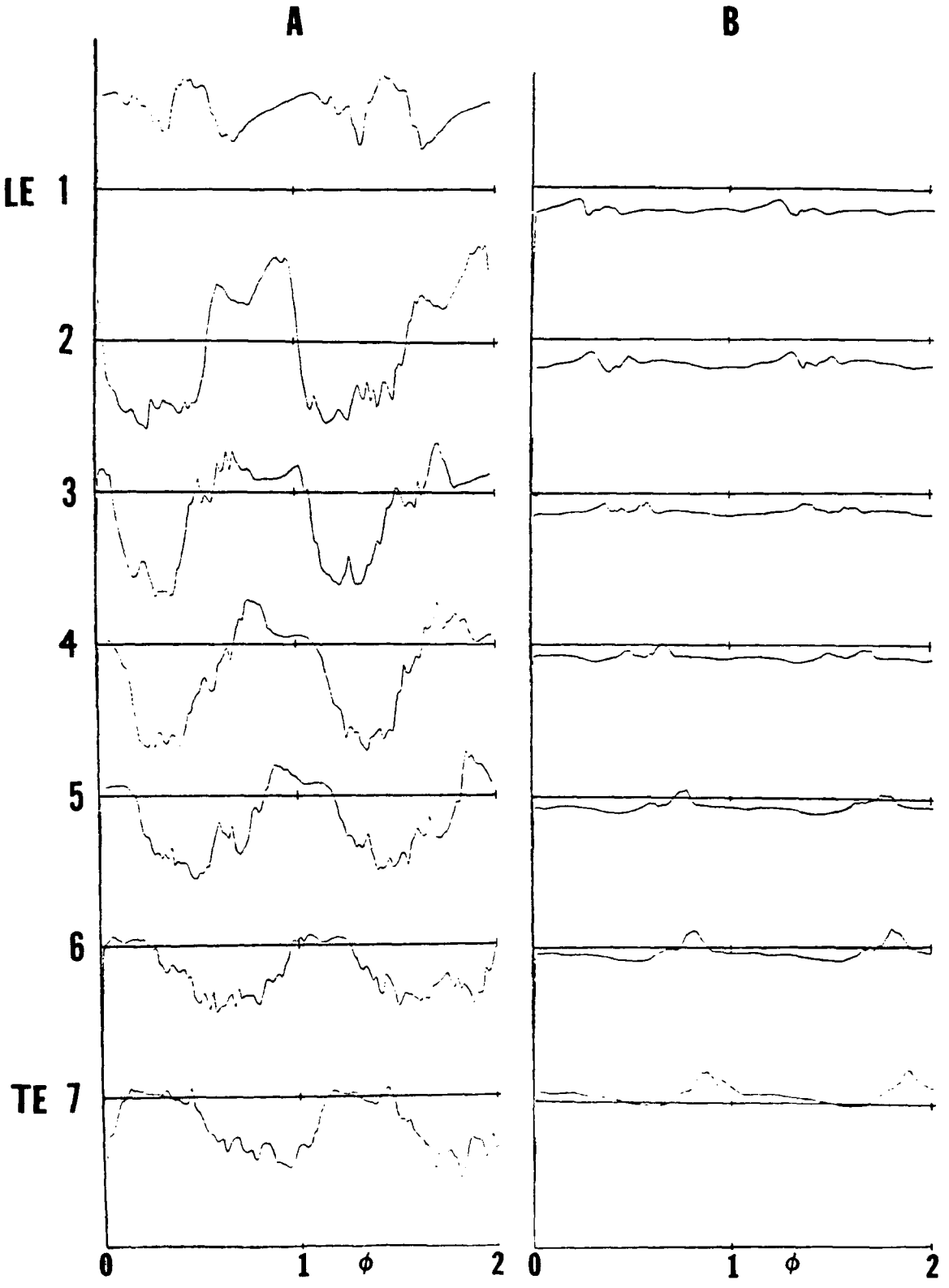

Fig. 4 Two-cycle velocity plots for flow about the wing in plane with the canard tip, 1-7: leading edge-trailing edge, A: plane one inch above the wing leading edge, B: plane one inch below the wing leading edge.

a separation bubble seen on the wing top surface in the time-synchronized photographs. The flow re-attaches in the aft portion of the wing and the recorded velocities once again show values close to freestream velocity. The lower surface velocities recorded simultaneously at this and all other data taking stations are only slightly changed by the cyclic flow produced by the motion of the canard.

The full-cycle flow influences produced by unsteady canard motions can only be illustrated with the velocity profiles at each hotwire probe station for the complete pitching cycle. Composite profiles are shown in Fig. 4 for the vertical plane at the canard tip and horizontal planes one inch above and one inch below the wing leading edge. The velocity profiles for two complete canard pitching cycles, ϕ = 0.0 to 2.0, are illustrated for each chordwise hotwire probe station from wing leading to trailing edge. The baseline for each plot is the tunnel freestream velocity and the two-cycle averaged plots indicate the repeatability of the velocity data.

The left column of Fig. 4 shows velocity fluctuations for the top surface of the wing. In these plots, the velocity maxima and minima indicate the attached and separated flow regions, respectively. At the leading edge, the velocity recorded by the hotwire probe is consistently above the freestream value and shows fluctuations consistent with the time course of canard vortex passage. As probe stations aft of the leading edge are investigated, strong velocity peaks and valleys are observed to correspond to definite phases of the pitching cycle. At point 2, a velocity minimum is seen over the first half of the pitching cycle and then a higher-than freestream velocity plateau is recorded for the second half of the cycle. This characteristic velocity signature corresponds to separated flow and then to attached flow regimes as seen in the visualization photographs (Fig. 2). With points from 2 through 7 being examined, the velocity valley shifts to a later point in the cycle and the velocity peak appears in the earlier portion of the cycle (point 7). This shift in velocity signature matches the temporal delays of the canard tip flow convecting across the surface of the wing.

The right column of Fig. 4 depicts the velocity fluctuations one inch below the wing surface. These lower wing surface velocities tend to remain close to the freestream velocity. Only slight fluctuations occur when the passage of the split canard tip vortex passes beneath the wing surface. Similar to the top surface flow, the lower surface disturbance is observed early in the pitching cycle at probe positions near the leading edge of the wing and later in the cycle at positions further aft.

To illustrate the instantaneous velocity at each chord station from leading to trailing edge, a temporal cross-plot of velocities at each hotwire probe station is shown in Fig. 5. The velocities at one inch above the wing are shown for one point in the pitching cycle. These patterns indicate the regions of attached, high velocity flow as well as the regions of turbulent, separated flow across the chordlength of the wing. A decrease in velocity is seen in the midchord region for ϕ = 0.2 and is observed to move aft toward the trailing edge as the oscillation cycle progresses. These profiles indicate the cyclic nature of the velocity signature about the wing with the oscillation cycle of the canard.

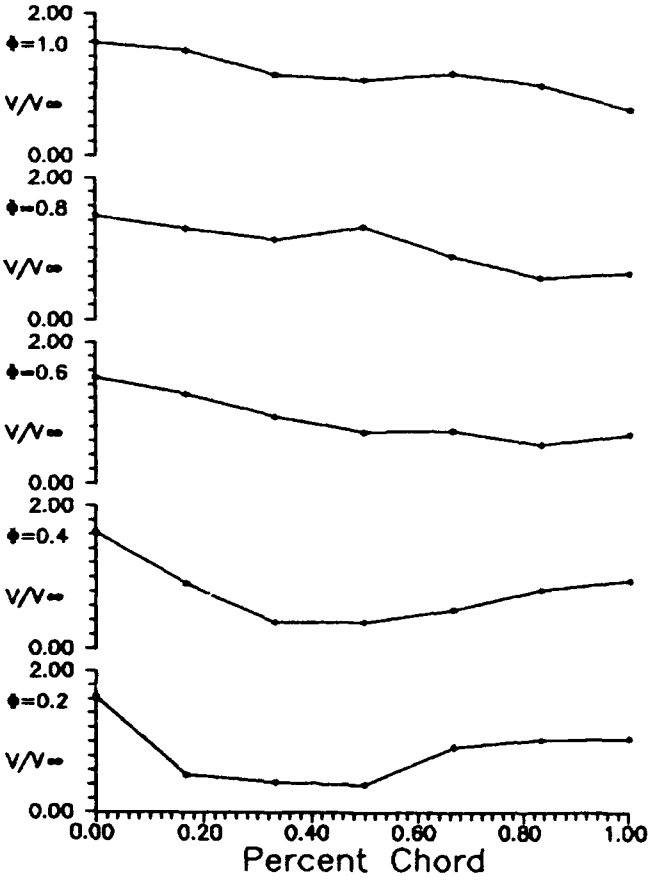

Fig. 5 Instantaneous velocity from leading edge to trailing edge, Vertical plane at canard tip, Horizontal plane at one inch above the wing, ϕ = 0.2 to 1.0.

The velocity fluctuations at the wing chord station of 0.167c (point 2 in Fig 4) are indicative of the patterns seen at the other chordwise locations. In this forward chordwise region, velocity has the most direct connection to the lift produced by the wing. For this reason, detailed analyses of the unsteady flow fields were accomplished at this chord location.

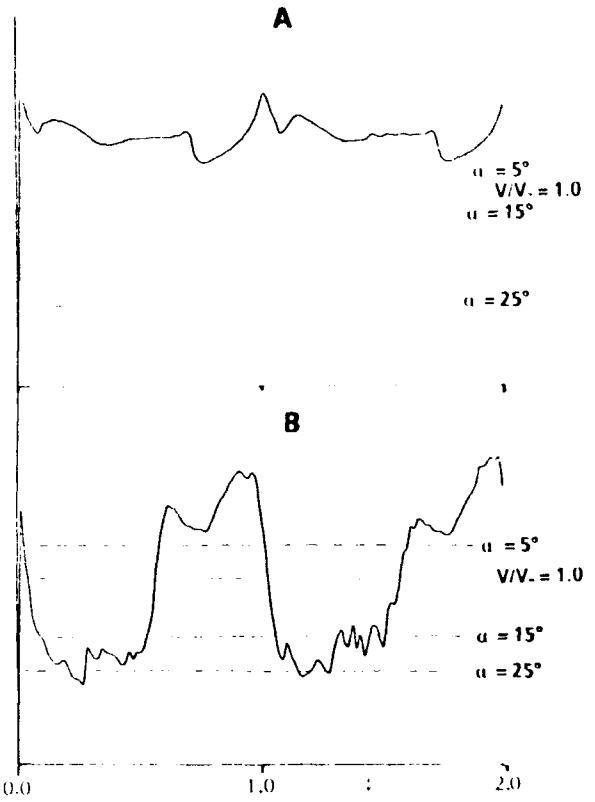

Fig. 6A/B Velocity profiles for the flow at 0.167c and horizontal plane one inch above the wing, A: vertical plane at canard midspan, B: vertical plane at canard tip.

Fig. 6A/B shows a complete velocity profile for the flow at one inch above the wing and at vertical planes behind the canard midspan and behind the canard tip. The velocity profiles shown throughout fluctuated above and below the freestream value and seem to indicate only rather nominal increases and decreases of flow speed. However, as is shown in Fig 6A/B these profiles are for a canard angle of attack varying between 5 degrees and 25 degrees. The velocity distributions for the static tests are shown as the solid lines on each figure. The velocities characteristic of low static angles of attack are elevated due to the attached flow about the canard and the subsequent canard downwash influence on the wing. As the static canard angle of attack is increased, the velocities at the wing surface decrease due to the turbulent separation behind the canard. Average velocity profiles for such dynamic tests are consistently above the static values for most canard angles of attack.

Figure 6A/B also illustrates the difference in dynamic velocity profiles between vertical planes behind the canard midspan and the canard tip. The profiles aft of the canard midspan show smaller velocity fluctuations than those aft of the canard tip. The average velocity behind the canard midspan is greater than the average value behind the canard tip. From the flow visualization photographs, the fluctuations aft of the canard tip are influenced by the cyclic canard tip vortex while the canard leading edge vortex passes well above the top surface of the wing and has little cyclic effect on the wing that is behind the canard midspan.

To determine the potential utility of applying forced sinusoidal oscillations to actual flight vehicles, investigations were performed using small amplitude oscillations of ± 2 degrees. A flow visualization comparison between static and dynamic results is shown in Fig. 7. The left column is for fixed angle of attack of the canard while the right column is for the oscillating canard with instantaneous angles of attack coinciding with those of the right column. The static data shows a separation bubble forming on the top surface of the canard with increased separation for the higher angles of attack. The dynamic data shows a region of dynamic stall vortex formation. The overall comparison implies more attached flow occurs over the oscillating canard even at only ± 2 degrees amplitude. The presumed lift enhancement from the dynamic stall vortex can only be verified by surface pressure measurements on the canard upper surface.

The effects of these small amplitude oscillations on the tandem wing are seen as velocity differences over the wing upper surface. A velocity profile plot for this oscillation amplitude at a chord location of 0.167c, similar to Fig. 6, reveals a significant velocity increase at the wing for the dynamic tests. An average velocity for one dynamic pitching cycle is $1.039V_\infty$ while the static average was only $0.717V_\infty$. The maximum and minimum velocities for the dynamic tests were 1.166 and 0.884, respectively. Each of these dynamic values are above the average, static canard velocities.

DISCUSSION

The complex three-dimensional flow patterns about the X-29 model are verified by both flow visualization and hotwire anemometry techniques. When the canard is oscillated through sinusoidal motions, the flow visualization photographs indicate attached flow about the canard throughout a wide range of angles of attack even those well above the normal static stall angles. This indicates an aerodynamically beneficial effect of the unsteady motions. However, the canard leading edge and tip vortices that enhance the flow on the canard are also shed from the canard surface and affect the flow about the tandem wing. This investigation partially demonstrates the effects and the sphere of influence of the unsteady flow structure produced about the wing. The study is

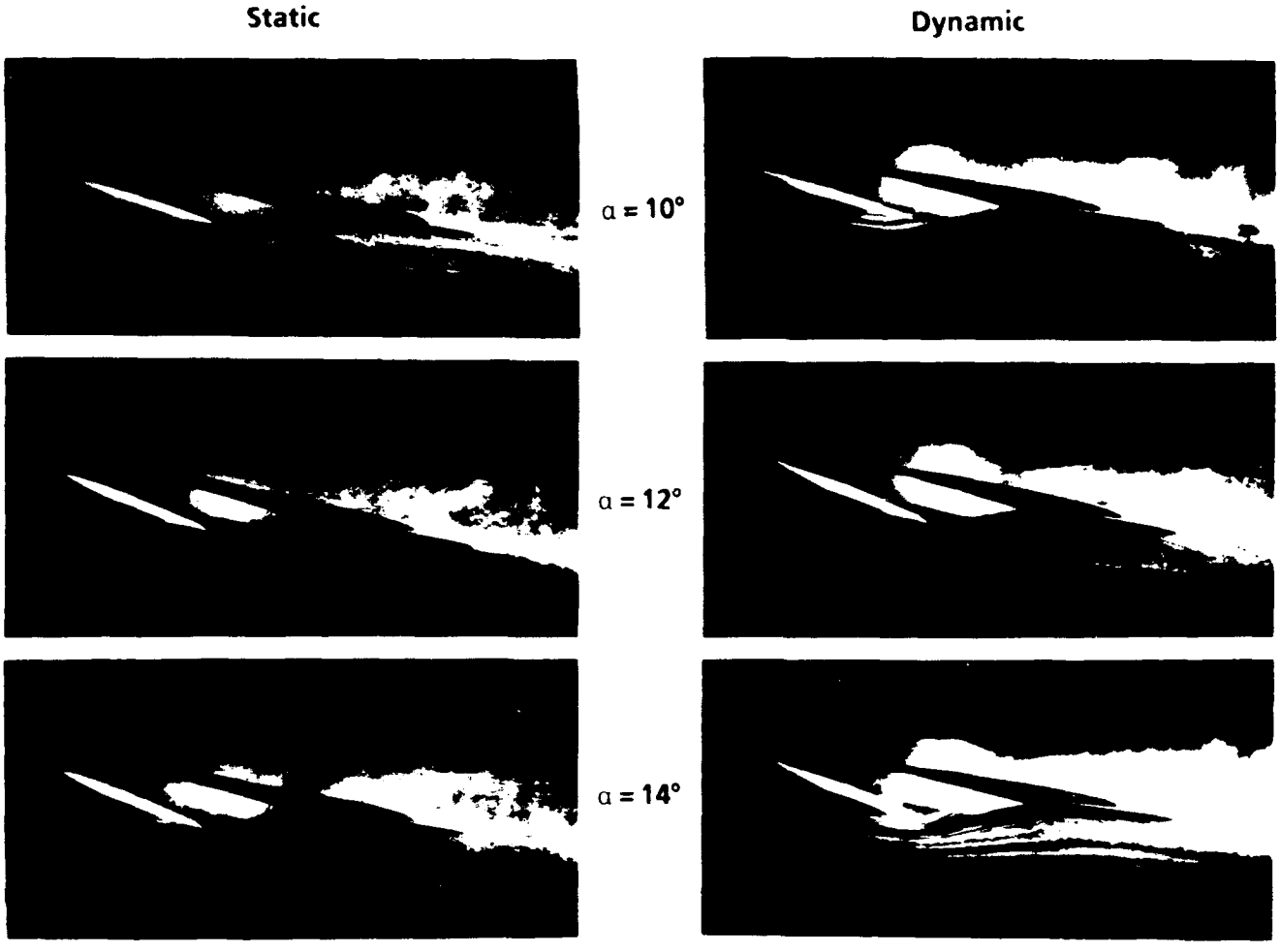

Fig. 7 Static and dynamic visualization comparisons for low amplitude oscillations, α = 10-14 degrees, α_m = 12 degrees, α_ω = ±2 degrees.

limited somewhat by the number of data planes investigated and the hotwire data sensing only the magnitude of normal velocities and not those of flows having other directional components.

The complex flow structure about both the canard and the wing is captured visually for one complete oscillation cycle in Fig. 2. This depiction with the data plane at the canard tip shows the dominance of the canard tip vortex early in the pitching cycle and, as the canard reaches lower angles of attack, the leading edge vortex becomes the prevailing structure. As the canard tip and leading edge vortices shed from the canard surface and interact with the wing leading edge, the flow patterns about the wing become cyclic and three-dimensional. The canard tip vortex is split by the leading edge of the wing and part of this rotational structure is observed passing above and below the wing. The above-wing portion causes locally increased effective angles of attack in the span region of the data plane. This increased angle of attack causes increased flow separation near the leading edge of the wing and the ensuing turbulent region traverses across the top surface of the wing. The under-wing portion of the canard tip vortex appears turbulent with little structural cohesion as it traverses the lower surface. The core of the canard leading edge vortex appears connected to the core of the canard tip vortex. Therefore, as the canard tip vortex is shed from the surface of the canard, the canard leading edge vortex follows and transverses across the surface of the wing immediately following the canard tip vortex. The leading edge vortex, however, passes well above the top surface of the wing and from the flow lines between the vortex and the surface of the wing appears to have little influence on the flow near the surface. To analyze the effects of the vortical structures as they pass across the wing surface, velocity and flow visualization comparisons are necessary.

The flow visualization and hotwire velocity comparison shown in Fig. 3 supports hypotheses formed from the visualization data. The velocity

variation for the probe positions near the leading edge of the wing range from greater than 1.5 times the freestream velocity to less than 0.5 times this baseline velocity value. The separation regions observed about the wing in the visualization photographs are quantified in the cyclic velocity data. The canard tip vortex produces locally high effective angles of attack of the wing and, consequently, flow separation which decreases the velocity. As the cyclic canard tip vortex passes aft across the surface of the wing, the velocity increases to a higher-than-freestream value. The canard leading edge vortex shows little influence on the velocity at the wing data planes of one inch and two inches above the surface. This must be due to the spatial distance of the canard leading edge vortex above the surface of the wing. The portion of the canard tip vortex that passes below the wing surface is discernible, but seems to have little influence on the lower surface flow.

The cyclic, complete velocity profiles of Fig. 4 illustrate the velocity peaks and valleys produced about the wing by the passage of the canard vortices. The upper-surface plots indicate high and low velocities which are not continuous across the chord of the wing. At one particular point in the pitching cycle, low velocities exist near the leading edge of the wing and higher velocities (near freestream) occur over the aft portion of the wing. These differential high and low velocity regions could cause pressure distributions about the wing which would produce cyclic pitching moments on the wing. The influence of these moments and the regional effects can only be determined by pressure distribution plots about the wing.

When the data plane is positioned at the canard midspan, Fig. 6A, the velocity data show little influence of the passage of the canard leading edge vortex across the surface of the wing. In this more inboard region, the canard tip vortex does not significantly affect the flow about the wing. The canard leading edge vortex must pass across the wing surface at this span location but the spatial distance between the vortex and the wing surface prevents any dominant effect of this vortex on the wing. The average velocity for the dynamic test is well above the static velocities at all angles of attack traced by the cyclic motion. This confirms the downwash effect from the canard when the flow is attached throughout the pitching cycle. The attached flow on the canard causes canard downwash which decreases the effective angle of attack of the tandem wing. A region of separated flow behind the fixed angle canard increases with increased static angle of attack. This separation from the canard causes somewhat turbulent and lower velocity flow at the wing surface.

The velocity fluctuations observed in Fig 6B at the span location aft of the canard tip are of greater magnitude than those seen at the more inboard location. These magnitude fluctuations indicate a stronger influence of the canard tip vortex when compared to the canard leading edge vortex as the vortical structures pass about the surface of the wing. Similar to the more inboard data, the velocities for the static tests decrease with increased fixed angle of attack of the canard. The average velocity for the dynamic test is still larger than for a fixed angle equal to the mean angle for oscillation.

Since large amplitude motions of a control surface may be structurally unsafe and extremely difficult to control, the feasibility of application of unsteady flow technology to an actual aircraft is shown in the small amplitude oscillation tests. The flow visualization photographs show an increased flow attachment for the dynamic tests. This attachment and leading edge vortex effect will enhance the lifting capability of the canard. The downwash created by the attached flow over the canard also causes the velocity over the surface of the tandem wing to be higher and therefore produces a greater lift on the wing.

CONCLUSIONS

The complex geometry of the X-29 model creates unique flow patterns about the lifting and control surfaces. The canard is tapered and, therefore, produces unsteady flow patterns similar to those characteristic of aft swept wings driven through identical dynamic motions[10]. As the canard is oscillated through sinusoidal motions, cyclic canard tip and leading edge vortices are formed. Flow visualization techniques illustrate a connection between the rotational cores of these two vortical structures, which is predicted by and satisfies Helmholtz's laws[18].

The hotwire velocity data recorded about both top and bottom surfaces of the wing confirm hypotheses formed during earlier flow visualization experiments. In the vertical plane behind the dynamic canard tip, more extreme velocity fluctuations exist on the wing than in the plane behind the canard midspan. This is due to the canard tip vortex impinging the surface of the wing while the canard leading edge vortex passes well above the upper surface of the wing. At a model angle of attack of zero, the leading edge vortex may have more effect on the flow about the wing. However, aircraft do not maneuver at zero angles of attack so enhancement of lift on a tandem wing from a leading edge vortex produced on a forward control surface cannot be ensured. The downwash produced by attached flow

over an oscillating forward surface increases the velocities about a trailing wing and seems to increase the lift producing capability of the wing. Therefore, producing forced unsteady oscillations of a control surface near the static stall for that surface appears to be a valid application of this unsteady flow phenomenon.

The geometry-dependent, three-dimensional flow patterns about the X-29 model are complex and somewhat difficult to analyze. The isolation of one or two independent flow parameters and the effects of these parameters on the overall flow patterns is, at best, perplexing. Therefore, to investigate the effects of forced unsteady flows produced about this model, comparisons must be made between the visualized data recorded by photography and the results obtained by hotwire anemometry. Even these techniques still leave some unanswered questions and ongoing investigations which include surface pressure measurements will more clearly define the unsteady flow fields about this model. The current investigations do provide, however, an insight into the behavior of unsteady flow structures about an actual aircraft model. Since maneuvering aircraft nearly always fly in an unsteady flow regime, a thorough comprehension of the characteristics of unsteady interactive flows is essential for the possible application of such phenomena.

ACKNOWLEDGMENTS

This work is supported, in part, by the U.S. Air Force Office of Scientific Research, Captain Hank Helin, project manager. The technical assistance of W. Bank, R. Meinzer and S. Huyer is appreciated.

REFERENCES

1. McCroskey, W.J., "Unsteady Airfoils," Annual Review of Fluid Mechanics, 1982, pp. 285-311.

2. Luttges, M.W., Robinson, M.C. and Kennedy, D.A., "Control of Unsteady Separated Flow Structures on Airfoils," AIAA-85-0531, AIAA Shear Flow Control Conference, Boulder, Colorado, March 1985.

3. Robinson, M.C. and Luttges, M.W., "Unsteady Flow Separation and Attachment Induced by Pitching Airfoils," AIAA-83-0131, AIAA 21st Aerospace Sciences Meeting, Reno, Nevada, Jan. 1983.

4. Helin, H.E., Robinson, M.C. and Luttges, M.W., "Visualization of Dynamic Stall Controlled by Large Amplitude Pitching Motions," AIAA-86-2281-CP, AIAA Atmospheric Flight Mechanics Conference, Williamsburg, Virginia, Aug. 1986.

5. Reisenthel, P.H., Nagib, H.M. and Koga, D.J., "Control of Separated Flows Using Forced Unsteadiness," AIAA-85-0556, AIAA Shear Flow Control Conference, Boulder, Colorado, March 1985.

6. Reynolds, W.C. and Carr, L.W., "Review of Unsteady, Driven, Separated Flows," AIAA Shear Flow Control Conference, Boulder, Colorado, March 1985.

7. Adler, J.N. and Luttges, M.W.,"Three-Dimensionality In Unsteady Flow About a Wing," AIAA-85-0132, AIAA 23rd Aerospace Sciences Meeting, Reno, Nevada, Jan. 1985.

8. Ashworth, J. and Luttges, M.,"Comparisons in Three-Dimensionality in the Unsteady Flows Elicited by Straight and Swept Wings," AIAA-86-2280CP, AIAA Atmospheric Flight Mechanics Conference, Williamsburg, Virginia, August 1986.

9. Ashworth, J., Waltrip, M. and Luttges, M.,"Three-Dimensional Unsteady Flow Fields Elicited by a Pitching Forward Swept Wing," AIAA-86-1104, AIAA 4th Joint Fluid Mechanics, Plasma Dynamics and Lasers Conference, Atlanta, Georgia, May 1986.

10. Ashworth, J., Huyer, S. and Luttges, M.,"Comparisons of Unsteady Flow Fields about Straight and Swept Wings Using Flow Visualization and Hotwire Anemometry," AIAA-87-1334, AIAA 19th Fluid Dynamics, Plasma Dynamics and Lasers Conference, Honolulu, Hawaii, June 1987.

11. Freymuth, P., Finaish, F. and Bank, W., "Visualization of Wing Tip Vortices in Accelerating and Steady Flow," Journal of Aircraft, Vol. 23, No. 9, Sept. 1986, pp. 730-733.

12. Freymuth, P., "The Vortex Patterns of Dynamic Separation: A Parametric and Comparative Study," Progress in Aerospace Sciences, Vol. 22, 1985, pp. 161-288.

13. Gad-el-Hak, M. and Ho, C., "Three-Dimensional Effects on a Pitching Lifting Surface," AIAA-85-0041, AIAA 23rd Aerospace Sciences Meeting, Reno, Nevada, Jan. 1985.

14. Gad-el-Hak, M. and Ho, C.," Unsteady Vortical Flow Around Three-Dimensional Lifting Surfaces," AIAA Journal, Vol. 24, No. 5, pp. 713-721, May 1986.

15. Ashworth, J., Mouch, T. and Luttges, M., "Application of Forced Unsteady Aerodynamics to a Forward Swept Wing X-29 Model," AIAA 26th Aerospace Sciences Meeting, Reno, Nevada, Jan. 1988.

16. Moore, M. and Frei, D., "X-29 and Forward Swept Wing Aerodynamic Overviews," AIAA-83-1834, AIAA Applied Aerodynamics Conference, Danvers, Massachusetts, July 1983.

17. Robinson, M.C., Helin, H.E. and Luttges, M.W., "Control of Wake Structure

Behind an Oscillating Airfoil," AIAA-86-2282-CP, AIAA Atmospheric Flight Mechanics Conference, Williamsburg, Virginia, Aug. 1986.

18. Schlichting, H., Boundary Layer Theory, McGraw-Hill Book Company, Sixth Edition, 1968.